Pergamon

Int. J. Heat Mass Transfer. Vol. 38, No. 17, pp. 3241–3251, 1995

0017-9310/95 $9.50+0.00

0017-9310(95)00048-8

Direct numerical simulation of a turbulent open channel flow with passive heat transfer

D. M. LU and G. HETSRONI†

Department of Mechanical Engineering, Technion-Israel Institute of Technology, Haifa 32000, Israel

(*Received* 9 *August* 1994 *and in final form* 12 *January* 1995)

Abstract—Direct numerical simulation (DNS) of a fully developed turbulent flume flow with passive heat transfer is performed using the finite-difference method with 50 400 grid points. The bottom wall is heated at a constant rate. The Reynolds number, based on the flume depth and the bulk velocity, is 2855, and the Prandtl number is 0.72. The results are satisfactory, and the comparison between the present results and those of other DNS investigations shows distinctive differences in the near-wall region owing to the difference in the thermal boundary conditions.

1. INTRODUCTION

With the advent of high-speed large-memory supercomputers, direct numerical simulation (DNS) of turbulent flow and heat transfer, i.e. solving turbulent flow and heat transfer problems directly from time-dependent three-dimensional Navier–Stokes and energy equations without any closure modeling of any turbulent scales, has become possible and drawn growing interest.

The role of DNS has been established as an important tool in studying the basic physics of turbulence, though the published DNS studies, especially those on turbulent heat transfer, are still relatively few in the literature; and the flows which may be investigated by DNS are currently limited to moderate Reynolds and Prandtl numbers due to the resolution barrier.

A major area in which DNS has been applied is the turbulent flows between two infinite parallel flat walls (or sometimes simply referred to as turbulent channel flows). This is because of the simple flow geometry and the significant engineering applications of wall-bounded flows. As far as the DNS of heat transfer in turbulent channel flows is concerned, Kim and Moin [1] simulated the turbulent thermal field between two isothermal walls. Lyons *et al.* [2] investigated the turbulent heat transfer in a channel with the bottom wall heated and the top wall cooled at the same rate. Kasagi *et al.* [3] performed DNS of turbulent heat transfer between two channel walls both heated at the same rate. In [2] and [3] steady wall temperature was imposed in addition to the constant heat fluxes on the walls. Hence there were no temperature fluctuations on the walls in any of the above simulations.

The assumption of steady wall temperature might be an approximation under certain conditions. In some cases, however, wall temperature may fluctuate. Thermal streaky structures have been observed to exist also on the walls in the experimental investigations [4, 5], in [5] an open channel water flow was heated at the bottom wall with a constant heat flux. For such cases, previous simulation studies might not capture certain physics because of the thermal boundary conditions. Hence an investigation on the turbulent heat transfer in which there are no restrictions on the wall-temperature fluctuation is certainly of intense interest from either a scientific or an engineering point of view. For instance, a knowledge of the temperature fluctuation on wall surfaces may be desirable in order to avoid thermal fatigue failure of certain solid structures.

Another matter which may be of interest concerns the numerical methods used for DNS studies. Although there are two major methods available, i.e. spectral methods and finite-difference methods, finite-difference methods have practically been ignored except for large eddy simulations. The fact that all the above-mentioned DNS studies used spectral or pseudo-spectral methods reflects on the popularity of spectral methods in the DNS community. Spectral methods have been favored as they are expected to be more accurate than finite-difference methods. However, spectral methods have their disadvantages in comparison with finite-difference methods, i.e. they are complex and inflexible with respect to flow geometry and boundary conditions. This is the main reason why the DNS studies have so far been restricted to flows with simple geometries such as plane channel flows. Schumann *et al.* [6] showed that only for very large numbers of modes is the accuracy of spectral schemes better than that of a second-order finite-difference scheme, and very often the numerical tests on the accuracy of the two methods have been undertaken using relatively coarse grids for simpler cases. Hence it may be reasonable to reckon that on a grid with resolution as fine as that required by DNS, the

† Author to whom correspondence should be addressed.

NOMENCLATURE

c_p	specific heat at constant pressure
h	heat transfer coefficient
k	thermal conductivity
Nu	Nusselt number $= 2h\delta/k$
Pr	Prandtl number $= \nu/\alpha$
Pr_t	turbulent Prandtl number $= \nu_t/\alpha_t$
p	pressure
q_w	wall heat flux
r	subdivision factor of geometric progression
R_{ij}	correlation coefficient $= \overline{u_i'u_j'}/u_{i\text{rms}}u_{j\text{rms}}$ or $= \overline{u_i'\theta'}/u_{i\text{rms}}\theta_{\text{rms}}$
Re_m	Reynolds number $= U_b 2\delta/\nu$
Re_δ	Reynolds number $= U_b\delta/\nu$
Re_τ	Reynolds number $= u_\tau\delta/\nu$
T	temperature
T_τ	friction temperature $= q_w/\rho c_p u_\tau$
t	time
U_b	bulk velocity
u_τ	friction velocity $= \sqrt{\tau_w/\rho}$
u, v, w	velocity components in the x, y and z directions
u_i	velocity component in the ith direction, u_1, u_2 and u_3 denote u, v and w, respectively
x, y, z	streamwise, normal and spanwise coordinates
x_i	coordinate in the ith direction, x_1, x_2 and x_3 denote x, y and z, respectively.

Greek symbols

α	thermal diffusivity $= k/\rho c_p$
α_t	eddy diffusivity for heat $= -\overline{v'T'}/(\partial\bar{T}/\partial y)$
δ	flume depth or depth of open channel flows
θ	temperature difference $= \langle T_w\rangle - T = \bar{T}_{p_w} - T_p$
ν	kinematic viscosity
ν_t	eddy viscosity $= -\overline{u'v'}/(\partial\bar{u}/\partial y)$
ρ	density
τ_w	average wall shear stress.

Superscripts and subscripts

$(\,)'$	fluctuating component
$(\,)^+$	normalized by the wall units, u_τ, ν and T_τ
$\overline{(\,)}$	ensemble average over the x–z plane and time
$\langle\,\rangle$	ensemble average over z direction and time
$(\,)_c$	value at the top surface of open channel flows
$(\,)_p$	periodic variable field
$(\,)_{\text{rms}}$	root-mean-square fluctuations
$(\,)_t$	turbulent process
$(\,)_w$	value at the wall.

difference between the numerical accuracy of the two methods may become negligible.

The major objectives of the present investigation are to simulate the characteristics of a fully developed turbulent open channel flow (motivated by [5]) with passive heat transfer under constant heat flux boundary conditions by using direct numerical simulation, and to explore the feasibilities of applying finite-difference schemes to DNS studies.

2. FORMULATION OF THE PROBLEM

The flow geometry and the coordinate system are illustrated in Fig. 1, in which u, v and w are the streamwise, normal and spanwise components of the fluid velocity, respectively; y denotes the distance from the bottom wall, and δ is the fluid depth. Constant heat flux q_w is input into the flow from the bottom wall and there are no restrictions on the wall temperature. The fluid is incompressible and has constant properties within the range of the field variables, with Prandtl number of 0.72.

The conservation equations of mass, momentum and energy for such a flow is quite standard and can be written as

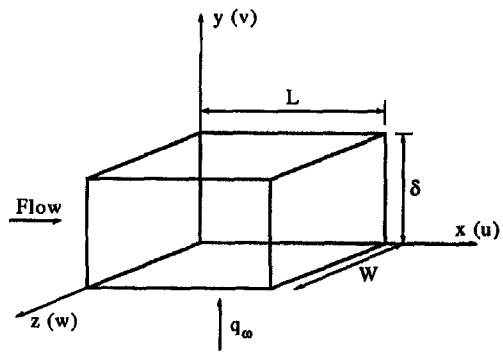

Fig. 1. Coordinate system and computational domain.

Mass equation
$$\frac{\partial u_i}{\partial x_i} = 0 \tag{1}$$

Momentum equation
$$\frac{\partial u_i}{\partial t} + \frac{\partial u_i u_j}{\partial x_j} = -\frac{1}{\rho}\frac{\partial p}{\partial x_i} + \frac{\partial}{\partial x_j}\left(\nu\left(\frac{\partial u_i}{\partial x_j} + \frac{\partial u_j}{\partial x_i}\right)\right) \tag{2}$$

Energy equation
$$\frac{\partial T}{\partial t} + \frac{\partial u_j T}{\partial x_j} = \frac{\partial}{\partial x_j}\left(a\frac{\partial T}{\partial x_j}\right). \tag{3}$$

The boundary conditions

Periodic boundaries are imposed in both streamwise and spanwise directions, and it is assumed that both hydro- and thermo-fields have the same periodic length in the same direction; the top surface is treated as a symmetry plane for both flow and thermal fields; and there is neither velocity slip on the wall surface, nor restriction on wall-temperature fluctuation.

In order to apply streamwise periodicity, the following transformations of the pressure and temperature have to be made because of the mean pressure and temperature gradients in the x-direction, i.e.

$$p = p_p - \left|\frac{d\langle p\rangle}{dx}\right| x \tag{4}$$

$$T = T_p + \left|\frac{d\langle T\rangle}{dx}\right| x \tag{5}$$

where p_p and T_p represent the periodic fields, $|d\langle p\rangle/dx|$ is estimated at a nominal Reynolds number by using the Blasius equation, and $|d\langle T\rangle/dx|$ is given by

$$\left|\frac{d\langle T\rangle}{dx}\right| = \frac{q_w}{\rho c_p U_b \delta} \tag{6}$$

where U_b is the bulk velocity.

Substituting equations (4) and (5) into equations (2) and (3) respectively, a new set of governing equations is derived, and the solutions to the new set of equations yield the u_i ($i = 1, 2, 3$), p_p and T_p fields.

The initial conditions are the mean profiles for u, v and w superimposed with sinusoidal perturbations and a uniformly distributed temperature field. However, the energy equation is not solved until the hydro-fields have reached a statistically steady state.

3. COMPUTATIONAL DOMAIN AND GRID SPACING

The choice of the size of the computational domain as illustrated in Fig. 1 is guided by the experience gained from previous DNS studies, e.g. those of Kim *et al.* [7] and Lam [8] and also by our experimental set-up. As mentioned earlier, the present investigation was motivated by our experimental investigation on the thermo-field structures in an open channel flow, which had been conducted in our group and where the thermal streaks had been observed on the heating wall [5]. Another consideration is to reduce the size of the computational domain as far as possible while observing the well-known two-point correlations. Hence the computational domain, $L \times W \times \delta$, is chosen to be $2\pi\delta \times \pi\delta \times \delta$.

The computation is carried out with 50400 grid points ($36 \times 20 \times 70$, in x, y, z) for a nominal Reynolds number, $Re_\delta = 3000$, which is based on U_b and δ. The estimated Re_τ, based on the wall friction velocity u_τ and δ, is 184, this gives an estimated computational domain in wall units (ν, u_τ, T_τ) as $L^+ \times W^+ \times \delta^+$, $1156 \times 578 \times 184$.

The grid spacings in the streamwise and spanwise directions are uniform and estimated as $\Delta x^+ \approx 32$ and $\Delta z^+ \approx 8$, respectively. Geometric progression (i.e. $\Delta y^+_{i+1} = r\Delta y^+_i$ where r is chosen to be 1.25) is used to generate non-uniform grids in the normal direction with grid spacing varying from about 0.4 next to the wall to about 20 near the symmetry plane or the interface of an open channel flow; there are about four grid points in the viscous sub-layer. The present grid spacing is definitely coarser than that of Kim *et al.* [7], who used $\Delta x^+ \approx 12$, $\Delta z^+ \approx 7$ and Δy^+ varying from 0.05 to 4.4, but is close to that of Lam [8], who used $\Delta x^+ \approx 33$, $\Delta z^+ \approx 8.4$ and Δy^+ varying from 0.1 next to the wall to 4.2 near the center of the flow. Although the estimated Kolmogorov scale in wall units is about 2, the turbulence statistics, to be presented below, indicate that no serious errors have been caused. Similar problem has been encountered by [7], [8] and others as well. The roles of these small eddies, if any, are still difficult to assess using today's technology. In our view, the relatively small eddies are most likely to be found in the near-wall region, and the tangible and important eddies in this region are known to be those associated with structures such as vortices, streaky structures, ejections and in-rush motions, which usually have sizes ranging from 10–100 (in planes perpendicular to the streamwise direction) to several hundreds (in the streamwise direction) in the wall units. Hence if these structures can be captured with reasonable resolution, then the simulation may be expected to be close to the reality.

4. NUMERICAL METHODS AND PROCEDURES

The numerical calculations were performed using Harwell code CFDS FLOW-3D release 3.2.1, which provides a flexible framework of finite-difference schemes.

In the present investigation central differencing in space is used since it is the least dissipative scheme compared with the other schemes available. The use of other schemes led to rapid decay of the initial perturbations. SIMPLEC is chosen to solve the pressure–velocity coupling, which is a modified form of the SIMPLE algorithm; the linearized momentum and energy equations are solved using Stone's method [9]; while the pressure correction equation is solved using AMG (Algebraic Multi-Grid) [10].

As to the time-stepping, from the two available schemes the Crank-Nicolson method was chosen as it is more accurate and less dissipative, in theory, than fully implicit backward Euler differencing in time. A combination of fixed and adaptive time steppings are used to gain control over the time step so that equilibrium could be achieved at a relatively fast rate without compromising the convergence and numerical stability, and the span of the time step was varied from 0.002 s to 0.05 s during the simulation, with

smaller time step applied in the beginning of the simulation and adjusting its value automatically by judging the convergence behavior. Once the statistically steady state was reached, the time step was kept as 0.05 s, which is quite conservative.

The simulation was started with the initial conditions described previously, and the time integration was repeated for about 30 LETOT (large eddy turn over time, δ/u_τ) when the variable fields was judged to have reached an equilibrium state, and then the simulation was further continued for about 10 LETOT with data sampled at arbitrary intervals over the last 5 LETOT of the simulation. The data sampled were used to calculate the turbulence statistics as ensemble averages over the x–z plane and time.

It is worth mentioning that the numerical method used was examined against the exact solutions of steady 2-D laminar open channel flows on various grid systems. The accuracy of the numerical solutions were found to be sufficiently good even for grids with grid spacing coarser than the present grid system.

5. RESULTS AND DISCUSSION

Owing to the difference in thermal boundary conditions between the present simulation and previous DNS studies, the turbulence statistics of the present thermal field may not be completely comparable with the results obtained by the previous DNS. The literature on the experimental investigations on the turbulent heat transfer mechanisms in thermally fully developed channel flows, is scarce. Hence the reliability of the resolved thermal field as well as the accuracy of the present simulation are mainly demonstrated by the statistical results of the hydro-fields. The present thermal results are compared with other results where possible, either to show the credibility of the present simulation as a whole, or to display the different phenomena and mechanisms that emerged as a result of the thermal boundary conditions.

It should be pointed out that all the quantities presented herein are normalized by the wall units, unless otherwise stated, and these variables are designated by superscript $(\ )^+$.

5.1. *Turbulence statistics of the hydro-fields*

With a nominal $Re_\delta = 3000$ and the estimated $Re_\tau = 184$, the simulation yields $Re_\delta = 2855$ and $Re_\tau = 184.5$. The calculated skin friction coefficient, $C_f = \tau_w/\frac{1}{2}\rho U_b^2 = 8.806 \times 10^{-3}$, and the ratio of the maximum mean velocity to the bulk velocity, $\bar{u}_c/U_b$ is 1.167. These figures are in good agreement with the corresponding values of 8.43×10^{-3} and 1.16, which are evaluated using Dean's correlations, $C_f = 0.073 Re_m^{-0.25}$ and $\bar{u}_c/U_b = 1.28 Re_m^{-0.0116}$ respectively, where Re_m is based on U_b and 2δ.

The distribution of the mean streamwise velocity vs y^+ is shown in Fig. 2. It can be seen that the present profile of $\bar{u}^+$ is satisfactory, and it is also noted that Kim *et al.* [7] obtained a profile coincident with the Nikuradze log law in the log-law region, which is not shown here. Hence the present results of $\bar{u}$ are between those of Kim *et al.* [7] and those of Lam [8].

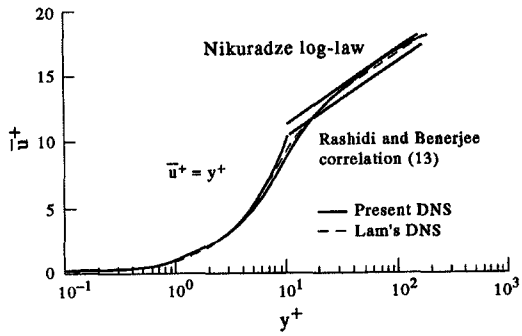

Fig. 2. Mean velocity profile.

Figure 3(a) and 3(b) present, respectively, the turbulence intensities and the Reynolds shear stress, calculated by the present simulation, along with some experimental data and the results obtained by other DNS studies. It is clear that the present results are parallel to other DNS results, which were obtained using spectral methods.

It is interesting to see that the present results appear to be in between those of Kim *et al.* [7] and Lam [8], who used spectral schemes and finer grids than the present one. This demonstrates the complexities associated with the DNSs of turbulent flows, which are highly non-linear and dynamic systems. The above comparisons primarily demonstrate that the present

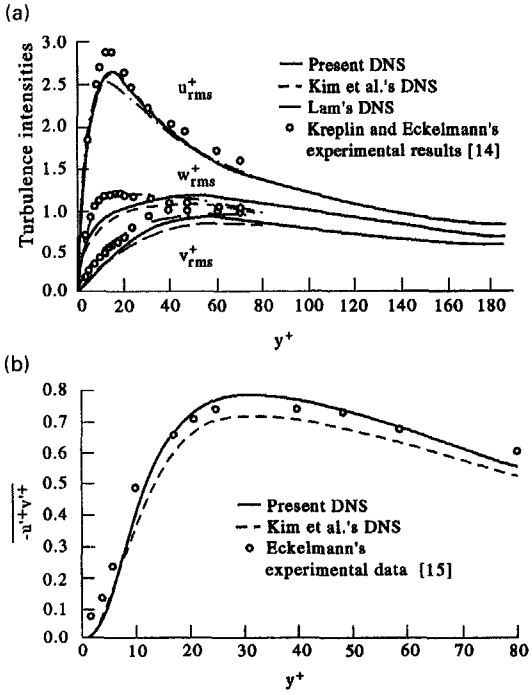

Fig. 3. Some fluctuating properties: (a) turbulence intensities; (b) Reynolds shear stress.

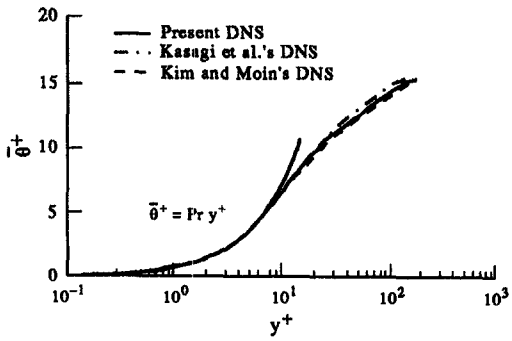

Fig. 4. Mean temperature profile.

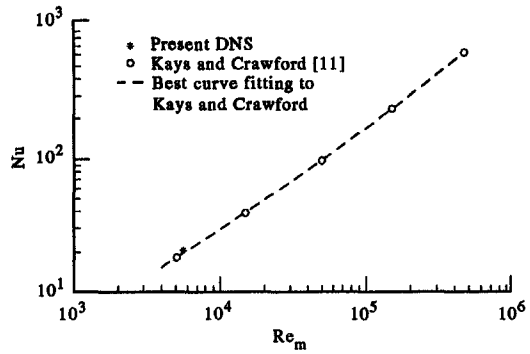

Fig. 5. Nusselt number for fully developed turbulent channel flows with a constant wall heat flux.

simulation, using finite-difference methods, has resolved all the important turbulent scales with satisfactory accuracy and may indicate that the differences between the accuracy of spectral methods and finite-difference methods become negligible when a very fine grid is used, which is a must for DNS studies. It may also be indicated that the difference in grid spacing between the present and other DNS studies is not substantial.

5.2. *Turbulence statistics of the thermal field*

In order to compare the present results of the thermal field with those of some other researchers, a transformation of the periodic T_p is required, which is written as

$$\theta = \bar{T}_{p_w} - T_p \tag{7}$$

or in the normalized form as

$$\theta^+ = (\bar{T}_{p_w} - T_p)/T_\tau. \tag{8}$$

Mean temperature profile, Nusselt number and temperature fluctuations. The mean temperature $\bar{\theta}^+$ distribution across the channel is shown in Fig. 4. The differences between the present DNS results and those of Kasagi *et al.* [3] and of Kim and Moin [1] may be caused by the different thermal boundary conditions but they could also result from the complexities associated with the numerical accuracy. All agree with the linear profile, $\bar{\theta}^+ = Pr\, y^+$ in the viscous sub-layer, i.e. $y^+ \leqslant 5$.

The Nusselt number obtained by the present simulation is 20.2, which is in good agreement with the value suggested by curve fitting to the experimental data of Kays and Crawford [11]. This is illustrated in Fig. 5.

The root-mean-square temperature fluctuations are compared with the results of Kasagi *et al.* [3]. As mentioned before, they also used isoflux thermal boundary conditions but imposed a non-fluctuating wall temperature. The comparisons are made vs y^+ and y/δ and are shown in Fig. 6(a) and 6(b), respectively. y is normalized by various scales to highlight the characteristics in different regions in the channel and also those resulting from the different Reynolds numbers, i.e. Re_τ.

It can be seen that there is a distinct difference between the present results and those of Kasagi *et al.* [3] in the near-wall region (e.g. $y^+ < 30$), where the temperature fluctuations obtained by the present simulation are much higher, in line with the wall-temperature fluctuation. Both simulations, however, calculate a maximum at about the same location ($y^+ \approx 18$) with the present maximum value being higher.

The wall-temperature fluctuation, which has not been reported by previous DNS studies, because of their thermal boundary conditions, corresponds to the wall thermal streaky structures. The typical wall-temperature pattern, obtained by the present simulation, is shown in Fig. 7(a). The pattern is seen to have streaky structure and is very similar to Fig. 7(b), which presents the wall thermal streaks observed in our experimental investigations using water as the working fluid. The mean spanwise spacing between

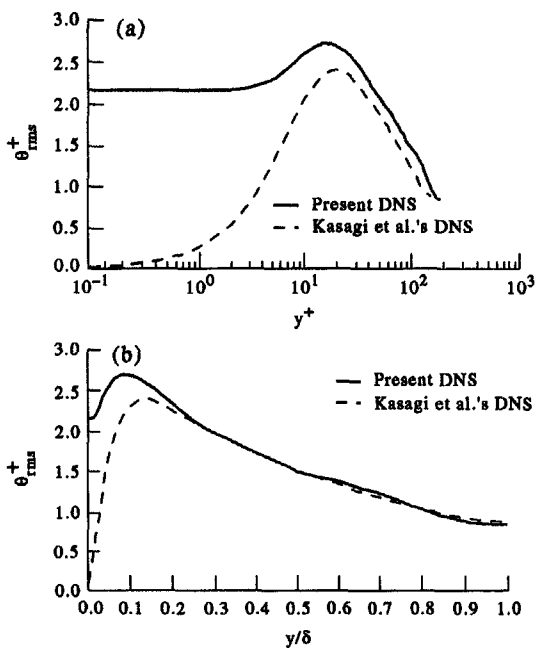

Fig. 6. Distribution of rms temperature fluctuations: (a) in wall coordinates; (b) in global coordinates.

the thermal streaks is about 110 by the present simulation, which is close to the well-known value of 100 for the spacing between low-speed streaks, while that obtained by the experiments [4] and [5] is about 80. We noticed that, due to the thermal resolution barrier posed by the relatively large Prandtl number of water, we were unable to simulate the experiments exactly in terms of Prandtl number and thus the Prandtl number simulated was changed to 0.72. However, we do believe that there should be at least a qualitative agreement between the present simulation and our experiments.

The simulated root-mean-square temperature fluctuations on the wall is about 13.6% of the temperature difference between the wall and fluid, $\Delta\bar{T}$, and the maximum wall-temperature fluctuation may reach as high as 42% of $\Delta\bar{T}$. The corresponding values obtained by the experimental investigation with a similar Reynolds number are 9–12% and 40%, respectively.

Figures 8 and 9 show the distributions of the streamwise and normal turbulent heat fluxes respectively. It is seen that the turbulent heat fluxes are markedly increased, especially in the near-wall region, because of the stronger temperature fluctuations there as a result of the present thermal boundary conditions.

The turbulent Prandtl number. The profile of the turbulent Prandtl number Pr_t, as calculated by the present simulation, is shown in Fig. 10(a). Also shown in Fig. 10(a) is Pr_t as obtained by Kasagi *et al.* [3]. It is interesting to see that the present turbulent Prandtl number in the viscous sub-layer is smaller than one, while Kasagi *et al.* [3] and also Kim and Moin [1] and Lyons *et al.* [2] have $Pr_t \approx 1$ in the region, as they all imposed steady wall temperature and thus had much smaller temperature fluctuations, which result in smaller turbulent heat fluxes in the near-wall region. The present value of Pr_t in the near-wall region, especially in the viscous sub-layer has, to our knowledge, not been reported before. It is also seen that the present Pr_t is smaller than that of Kasagi *et al.* [3] throughout the channel. As a result, the bulk turbulent Prandtl number obtained by the present simulation is about 0.75, which is smaller than 0.9, a value commonly used for turbulent heat transfer analysis.

It should be pointed out, however, that although the Pr_t is less than one in the viscous sub-layer, this does not have considerable effect on the mean temperature profile in the viscous sub-layer, as the turbulent heat flux is negligibly small compared with the molecular heat transfer in this region, which is demonstrated in Fig. 10(b).

Cross-correlation coefficients. Figure 11 shows the cross-correlation coefficients. It is seen that there is a general similarity between $-R_{uv}$ and $-R_{v\theta}$ caused by the strong correlation between u' and θ', which is demonstrated by the $R_{u\theta}$ profile. However, compared with the results of Kasagi *et al.* [3] results (not shown here), the present $R_{u\theta}$ is markedly smaller than the values simulated by them in the near-wall region, which indicates that u' and θ' are less correlated in this region in our case due to the stronger temperature fluctuation. Outside the near-wall region, the present results are close to those of Kasagi *et al.*; and both simulations have a maximum of $R_{u\theta}$ at about $y^+ \approx 8$–10.

The budgets for fluctuating and mean temperature variances. The advantages of DNS of turbulent flow and heat transfer lie in that it may provide various data, which may be difficult to obtain by experiments, thus giving a better understanding of the mechanisms of turbulent flow and heat transfer and making it possible to test and develop turbulent closure models. Very often, the budget equations for the fluctuating temperature variance and mean temperature variance are instructive in assessing the advantages.

The budget equation for the fluctuating temperature variance can be derived as

$$0 = \overline{u'^+\theta'^+}\left|\frac{\mathrm{d}\langle T\rangle^+}{\mathrm{d}x^+}\right| - \overline{v'^+\theta'^+}\frac{\mathrm{d}\bar{\theta}^+}{\mathrm{d}y^+} - \frac{1}{Pr}\overline{\frac{\partial\theta'^+}{\partial x_i^+}\frac{\partial\theta'^+}{\partial x_i^+}} - \frac{\mathrm{d}}{\mathrm{d}y^+}(\overline{v'^+\theta'^{+2}}/2) + \frac{1}{Pr}\frac{\mathrm{d}}{\mathrm{d}y^+}\left(\frac{\mathrm{d}\overline{\theta'^{+2}/2}}{\mathrm{d}y^+}\right). \quad (9)$$

The first two terms in equation (9) are the production of the turbulent fluctuating temperature; the third term is the dissipation of temperature fluctuations; the fourth term is the turbulent diffusion (TD) of temperature fluctuations by normal velocities; and the last term is the molecular diffusion (MD) of temperature fluctuations. Figure 12(a) presents the terms in equation (9) along with the experimental results obtained by Krishnamoorthy and Antonia [12]. They investigated the temperature dissipation of an air channel flow which was heated at a constant rate from the bottom aluminum floor, and there was supposed to be no wall-temperature fluctuation in their experimental setup. The typical uncertainties associated with their TD and dissipation data ranged from ± 0.01 to ± 0.03 in the vertical ordinate unit.

It can be seen that the agreement between the present simulation and the Krishnamoorthy and Antonia's [12] data is reasonably good except in the viscous sub-layer, where the present MD and dissipation terms are smaller than the experimental values. The deviations may be a result of the difference in the wall thermal boundary conditions. It should also be pointed out that the experimental data in the vicinity of the wall could possibly be subject to serious errors associated with X-probe measurement in the region.

Figure 12(b) shows [3] the DNS results of Kasagi *et al.* of each term in equation (9) together with Krishnamoorthy and Antonia's [12] data. Comparing with Fig. 12(a), it can be seen that the difference between the present budget terms and those of Kasagi *et al.* [3] occurs mainly in the vicinity of the wall, in particular in the viscous sub-layer, while outside this region, the two results are very close. Hence the influences of wall-temperature fluctuation appear to be limited to the near-wall region.

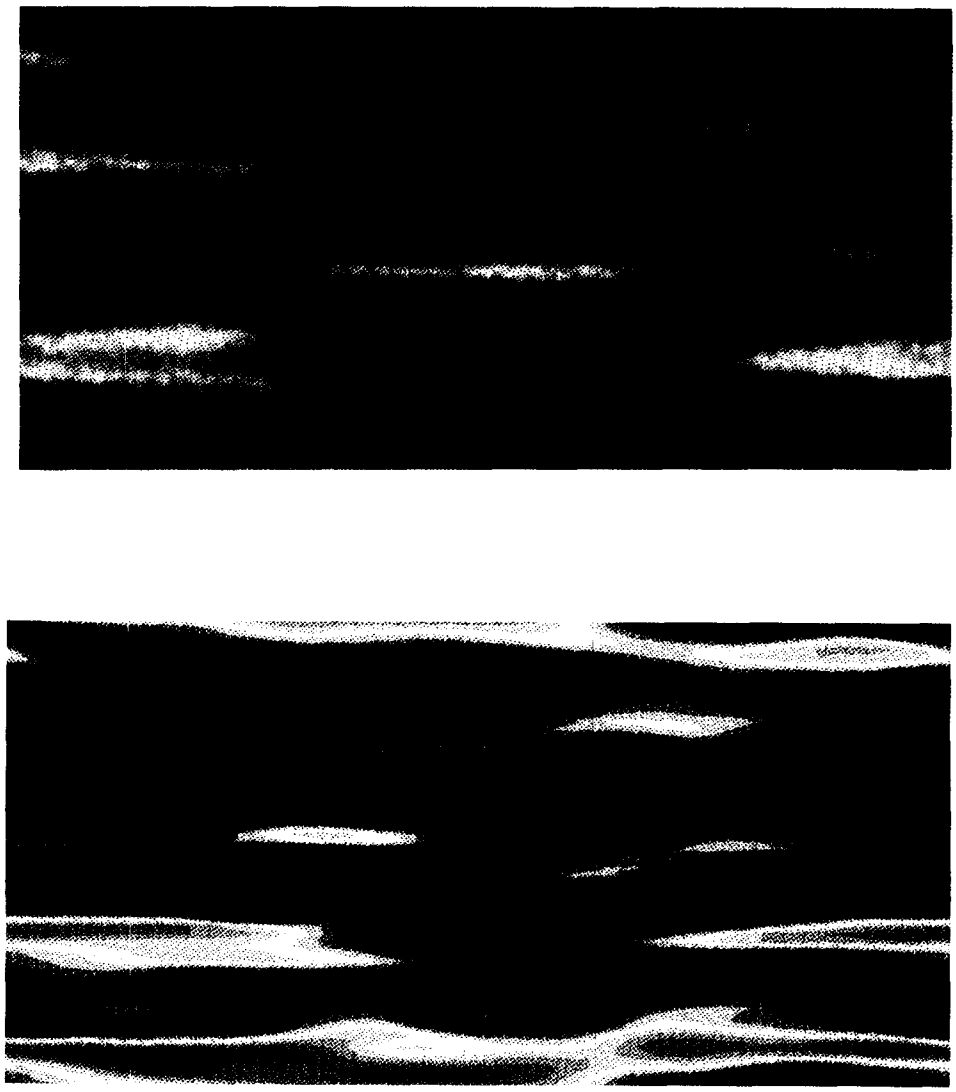

Fig. 7. Wall-temperature pattern (a) present DNS result; (b) experimental result [5].

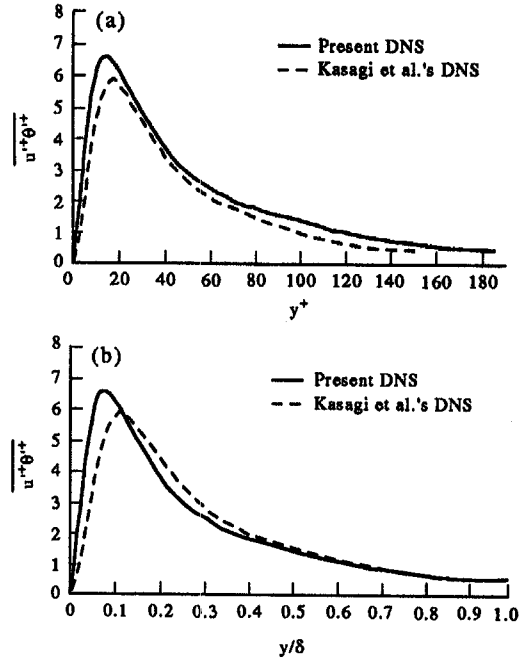

Fig. 8. Distribution of streamwise turbulent heat flux: (a) in wall coordinates; (b) in global coordinates.

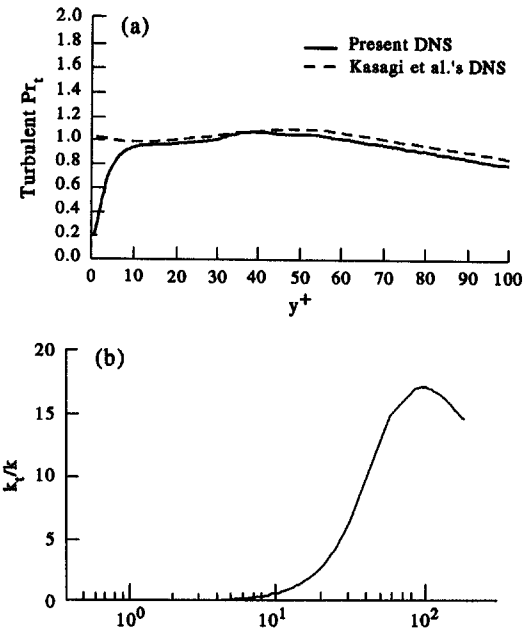

Fig. 10. Turbulent heat transport properties: (a) distribution of turbulent Prandtl number; (b) ratio of eddy to molecular thermal conductivity.

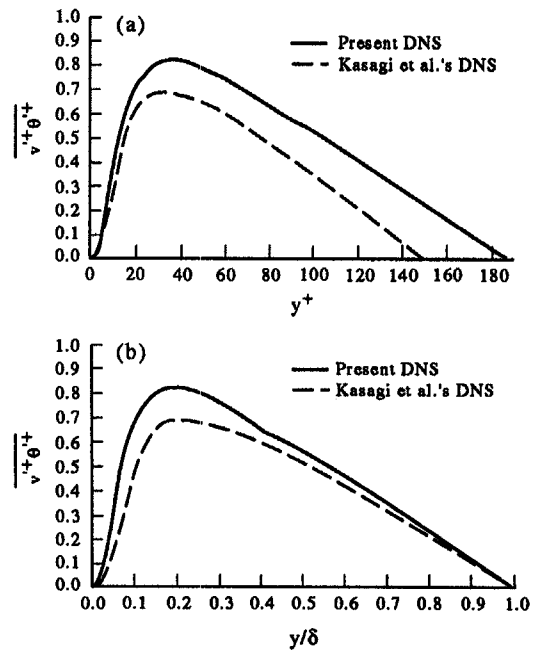

Fig. 9. Distribution of wall-normal turbulent heat flux: (a) in wall coordinates; (b) in global coordinates.

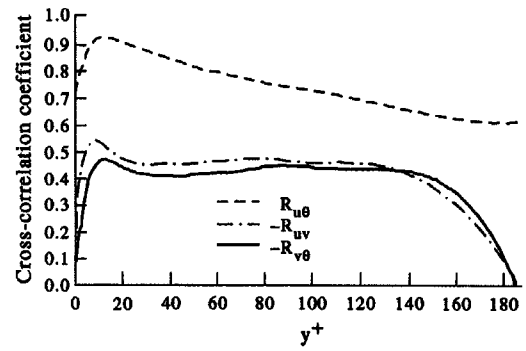

Fig. 11. Cross-correlation coefficients between u', v' and θ'.

It is also demonstrated in Fig. 12(a) that the production and the dissipation are the two largest terms in equation (9), and for $y^+ > 40$, production and dissipation are in local balance; while in the region $y^+ < 40$, the TD and MD redistribute temperature fluctuations and are most important in the region $y^+ < 15$.

The budget equation for the mean temperature variance displays the contributions of various processes to the macro-energy balance and reflects the interaction between the mean and the fluctuating processes. It is written as

$$0 = \bar{u}^+\bar{\theta}^+\left|\frac{\mathrm{d}\langle T\rangle^+}{\mathrm{d}x^+}\right| + \overline{v'^+\theta'^+}\frac{\mathrm{d}\bar{\theta}^+}{\mathrm{d}y^+} - \frac{1}{Pr}\left(\frac{\mathrm{d}\bar{\theta}^+}{\mathrm{d}y^+}\right)^2 - \frac{\mathrm{d}}{\mathrm{d}y^+}(\overline{v'^+\theta'^+}\bar{\theta}^+) + \frac{1}{Pr}\frac{\mathrm{d}}{\mathrm{d}y^+}\left(\frac{\mathrm{d}\bar{\theta}^{+2}/2}{\mathrm{d}y^+}\right). \quad (10)$$

The first term in equation (10) is the heat source caused by the wall heating; the second term is the production of turbulent fluctuating temperature variance, it is a loss term here but appears in equation (9) as a source term; the third term is the dissipation of the mean temperature variance; the fourth term

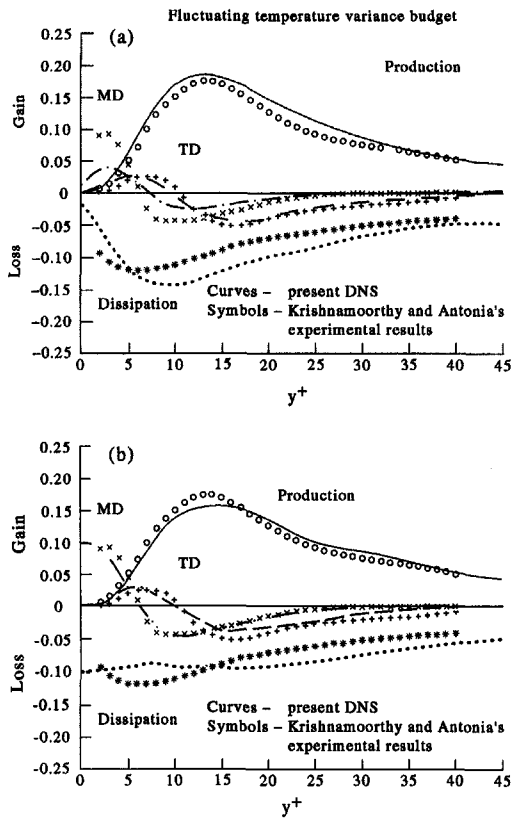

Fig. 12. Budget of the fluctuating temperature variance in the wall region: (a) present DNS vs experimental results [12]; (b) results of Kasagi *et al.* vs. experimental results [12].

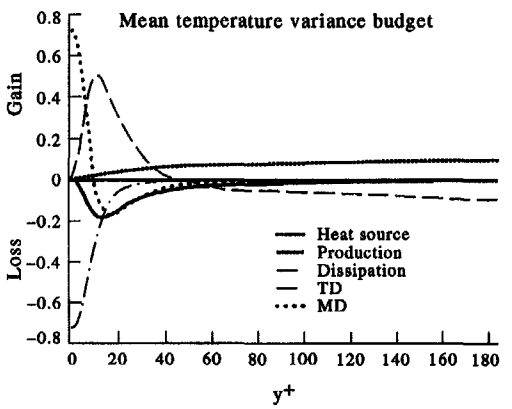

Fig. 13. Budget of mean temperature variance.

represents the turbulent diffusion of the mean temperature variance; and the last term gives the molecular diffusion of the mean temperature variance. All these terms, as were obtained by the present simulation, are shown in Fig. 13. As seen, the viscous dissipation is balanced by MD at the wall. In the buffer region, all the terms play important roles, and the turbulent thermal energy is mainly produced in this region by converting the mean thermal energy, which is transported by TD from the core $y^+ > 40$, into turbulent thermal energy. In the core, the heat source supplies the mean thermal energy, which is converted into turbulent thermal energy in the near-wall region.

6. CONCLUSIONS

Direct numerical simulation of a fully developed turbulent open channel flow, with a constant heat flux boundary condition, is performed for a fluid with a Prandtl number of 0.72 and Re_δ of 2855 using finite-difference schemes.

1. The turbulence statistics of both hydraulic and thermal fields are presented and compared with results obtained by others. The present simulation results are satisfactory and the accuracy appears to be just as good as those of previous DNS investigations using spectral methods, even though the computation is executed on a grid coarser than those used by other DNS researchers. This implies that the difference in the numerical accuracy between finite-difference methods and spectral methods may become negligible when fine grids, such as required by DNS, are used. The grid spacing may not necessarily be exactly the same as those used by other DNS studies in certain directions and regions because of the inhomogeneity and anisotropy of the turbulence structures, provided that the important turbulence structures are captured with reasonable resolution. Hence, finite-difference methods can be used for DNS studies. This conclusion may have significant implications for DNS studies of turbulent flows with complex geometries, namely, geometries that are more complex than plane channel may now be investigated using DNS with finite-difference schemes.

2. The Nusselt number calculated is 20.2, which is in good agreement with that suggested by Kays Crawford [11].

3. Distinctively different phenomena and mechanisms from those obtained by the previous DNS studies occur in the near-wall region, especially in the viscous sub-layer and buffer zone; this is because of the present thermal boundary condition.

(a) Wall thermal streaky structures, which have not been investigated by previous DNS studies, are closely resemble the flow structures in the near-wall region. The mean spanwise spacing between the thermal streaks is about 110. The root-mean-square temperature fluctuation on the wall is about 13.6% of the difference between the mean wall temperature and the fluid bulk temperature; the maximum amplitude of wall temperature fluctuations may be as high as 42% of the temperature difference between the heating wall and the fluid. Similar values of wall-temperature fluctuations were obtained experimentally in [5].

As consequences of the wall temperature fluctuation, temperature fluctuations and turbulent heat

fluxes are markedly increased in the near-wall region ($y^+ < 30$).

(b) The turbulent Prandtl number Pr_t is smaller than the Prandtl number in the immediate vicinity of the wall, especially in the viscous sub-layer, but the Pr_t obtained by other DNS studies is about one in the same region because of their steady wall temperature assumptions. The present bulk Pr_t is about 0.75, which is close to molecular Pr.

(c) The budget equation for fluctuating temperature variance shows different characteristics in the near-wall region from those of other DNS studies.

It appears that the impacts of the wall temperature fluctuation on turbulent heat transport characteristics are significant within the near-wall region.

Acknowledgements—This research is supported by a United States–Israel Binational Science Foundation Grant no 90-00428/1 and by the Basic Research Foundation administered by the Israel Academy of Science and Humanities. D. M. Lu is supported by a grant from the Israel Council of Higher Education. The authors also thank Dr I. P. Jones of Harwell for some discussion about the CFDS FLOW-3D.

REFERENCES

1. J. Kim and P. Moin, Transport of passive scalars in a turbulent channel flow. In *Turbulent Shear Flows VI* (Edited by J.-C. André *et al.*), pp. 85–96. Springer, Berlin (1989).
2. S. L. Lyons, T. J. Hanratty and J. B. McLaughlin, Direct numerical simulation of a passive heat transfer in a turbulent channel flow, *Int. J. Heat Mass Transfer* **34,** 1149–1161 (1991).
3. N. Kasagi, Y. Tomita and A. Kuroda, Direct numerical simulation of passive scalar field in a turbulent channel flow, *J. Heat Transfer, Trans. ASME* **114,** 598–606 (1992).
4. Y. Iritani, N. Kasagi and M. Hirata, Heat transfer mechanism and associated turbulence structure in the near wall region of a turbulent boundary layer, *4th Symposium on Turbulent Shear Flows*, pp. 17.31–17.36, Karlsruhe (1983).
5. G. Hetsroni and R. Rozenblit, Heat transfer to a liquid–solid mixture in a flume, *Int. J. Multiphase Flow* **20,** 671–689 (1994).
6. U. Schumann, G. Grötzbach and L. Kleiser, Direct numerical simulation of turbulence. In *Prediction Methods for Turbulent Flows* (Edited by W. Kollmann), pp. 123–258. Hemishpere, Washington, DC (1980).
7. J. Kim, P. Moin and R. Moser, Turbulence statistics in fully developed turbulent channel flow at low Reynolds number, *J. Fluid Mech.* **177,** 133–166 (1987).
8. K. L. Lam, Numerical investigation of turbulent flow bounded by a wall and a free-slip surface, Ph.D. dissertation, University of California at Santa Barbara, CA (1989).
9. H. L. Stone, Iterative solution of implicit approximations of multi-dimensional partial differential equations, *SIAM J. Num. Analysis* **7,** 104–111 (1968).
10. R. D. Lonsdale, An algebraic multi-grid solver for the Navier Stokes equations on unstructured meshes, *Int. J. Num. Meth. Heat Fluid Flow* **3,** 3–14 (1993).
11. W. M. Kays and M. E. Crawford, *Convective Heat and Mass Transfer* (2nd Edn), McGraw-Hill, New York (1980).
12. L. V. Krishnamoorthy and R. A. Antonia, Temperature dissipation measurements in a turbulent boundary layer, *J. Fluid Mech.* **176,** 265–281 (1987).
13. M. Rashidi and S. Benerjee, Turbulence structure in free-surface channel flows, *Phys. Fluids* **31,** 2491–2503 (1988).
14. H. Kreplin and H. Eckelmann, Behavior of the three fluctuating velocity components in the wall region of a turbulent channel flow, *Phys. Fluids* **22,** 1233–1239 (1979).
15. H. Eckelmann, The structure of the viscous sublayer and the adjacent wall region in a turbulent channel flow, *J. Fluid Mech.* **65,** 439–459 (1974).